# Single pulse coherence measurements in the water window at the free-electron laser FLASH

**D. D. Mai,[1] J. Hallmann,[3] T. Reusch,[1] M. Osterhoff,[1] S. Düsterer,[2] R. Treusch,[2] A. Singer,[2] M. Beckers,[5] T. Gorniak,[5,6] T. Senkbeil,[5,6] R. Dronyak,[2] J. Gulden,[2] O. M. Yefanov,[2] A. Al-Shemmary,[2] A. Rosenhahn,[5,6] A. P. Mancuso,[3] I. A. Vartanyants,[2,4] and T. Salditt[1,*]**

*1 Institute for X-ray Physics, Georg-August-University Göttingen, Germany*
*2 Deutsches Elektronen-Synchrotron, Hamburg, Germany*
*3 European XFEL GmbH, Hamburg, Germany*
*4 National Research Nuclear University, 'MEPhI', 115409 Moscow, Russia*
*5 Applied Physical Chemistry, Heidelberg, Germany*
*6 Analytical Chemistry - Biointerfaces, Ruhr-University Bochum, 44780 Bochum, Germany*

*tsaldit@gwdg.de*

**Abstract:** The spatial coherence of free-electron laser radiation in the water window spectral range was studied, using the third harmonic ($\lambda_{3rd} = 2.66$ *nm*) of DESY's Free-electron LASer in Hamburg (FLASH). Coherent single pulse diffraction patterns of 1,2-Dioleoyl-sn-glycero-3-phosphocholine (DOPC) multilamellar lipid stacks have been recorded. The intensity histogram of the speckle pattern around the first lamellar Bragg peak, corresponding to the $d = 5$ *nm* periodicity of the stack, reveals an average number of transverse modes of $\bar{M} = 3.0$ of the 3rd harmonic. Using the lipid stack as a 'monochromator', pulse-to-pulse fluctuations in the third harmonic $\lambda_{3rd}$ have been determined to be 0.033 *nm*.



**OCIS codes:** (030.0030) Coherence and statistical optics; (140.2600) Free-electron lasers (FELs);(160.1435) Biomaterials; (030.6140) Speckle.

## References and links

1. M. A. Le Gros, G. McDermott, and C. A. Larabell, "X-ray tomography of whole cells," Curr. Opin. Struct. Biol. **15**, 593–600 (2005).
2. G. Schneider, P. Guttmann, S. Heim, S. Rehbein, F. Mueller, K. Nagashima, J. B. Heymann, W. G. Müller, and J. G. McNally, "Three-dimensional cellular ultrastructure resolved by X-ray microscopy," Nat. methods **7**, 985–988 (2010).
3. K. Giewekemeyer, M. Beckers, T. Gorniak, M. Grunze, T. Salditt, and A. Rosenhahn, "Ptychographic coherent x-ray diffractive imaging in the water window," Opt. Express **19**, 1037 (2011).
4. W. Ackermann, G. Asova, V. Ayvazyan, A. Azima, N. Baboi, J. Bähr, V. Balandin, B. Beutner, A. Brandt, A. Bolzmann, R. Brinkmann, O. I. Brovko, M. Castellano, P. Castro, L. Catani, E. Chiadroni, S. Choroba, A. Cianchi, J. T. Costello, D. Cubaynes, J. Dardis, W. Decking, H. Delsim-Hashemi, A. Delserieys, G. Di Pirro, M. Dohlus, S. Düsterer, A. Eckhardt, H. T. Edwards, B. Faatz, J. Feldhaus, K. Flöttmann, J. Frisch, L. Fröhlich, T. Garvey, U. Gensch, Ch. Gerth, M. Görler, N. Golubeva, H.-J. Grabosch, M. Grecki, O. Grimm, K. Hacker, U. Hahn, J. H. Han, K. Honkavaara, T. Hott, M. Hüning, Y. Ivanisenko, E. Jaeschke, W. Jalmuzna, T. Jezynski, R. Kammering, V. Katalev, K. Kavanagh, E. T. Kennedy, S. Khodyachykh, K. Klose, V. Kocharyan, M. Körfer, M. Kollewe, W. Koprek, S. Korepanov, D. Kostin, M. Krassilnikov, G. Kube, M. Kuhlmann, C. L. S. Lewis, L. Lilje, T. Limberg, D. Lipka, F. Löhl, H. Luna, M. Luong, M. Martins, M. Meyer, P. Michelato, V. Miltchev, W. D. Möller, L. Monaco, W. F. O. Müller, O. Napieralski, O. Napoly, P. Nicolosi, D. Nölle, T. Nunez, A. Oppelt, C. Pagani, R. Paparella, N. Pchalek, J. Pedregosa-Gutierrez, B. Petersen, B. Petrosyan, G. Petrosyan, L. Petrosyan, J. Pflüger,

#186355 - $15.00 USD Received 8 Mar 2013; revised 11 Apr 2013; accepted 11 Apr 2013; published 20 May 2013

E. Plönjes, L. Poletto, K. Pozniak, E. Prat, D. Proch, P. Pucyk, P. Radcliffe, H. Redlin, K. Rehlich, M. Richter, M. Roehrs, J. Roensch, R. Romaniuk, M. Ross, J. Rossbach, V. Rybnikov, M. Sachwitz, E. L. Saldin, W. Sandner, H. Schlarb, B. Schmidt, M. Schmitz, P. Schmüser, J. R. Schneider, E. A. Schneidmiller, S. Schnepp, S. Schreiber, M. Seidel, D. Sertore, A. V. Shabunov, C. Simon, S. Simrock, E. Sombrowski, A. A. Sorokin, P. Spanknebel, R. Spesyvtsev, L. Staykov, B. Steffen, F. Stephan, F. Stulle, H. Thom, K. Tiedtke, M. Tischer, S. Toleikis, R. Treusch, D. Trines, I. Tsakov, E. Vogel, T. Weiland, H. Weise, M. Wellhöfer, M. Wendt, I. Will, A. Winter, K. Wittenburg, W. Wurth, P. Yeates, M. V. Yurkov, I. Zagorodnov, and K. Zapfe, "Operation of a free electron laser from the extreme ultraviolet to the water window," Nat. Photonics **1**, 336–351 (2007).

5. R. Akre, D. Dowell, P. Emma, J. Frisch, S. Gilevich, G. Hays, Ph. Hering, R. Iverson, C. Limborg-Deprey, H. Loos, A. Miahnahri, J. Schmerge, J. Turner, J. Welch, W. White, and J. Wu, "Commissioning the Linac Coherent Light Source injector," Phys. Rev. Spec. Top. Accel Beams **11**, 030703 (2008).
6. A. P. Mancuso, Th. Gorniak, F. Staier, O. M. Yefanov, R. Barth, C. Christophis, B. Reime, J. Gulden, A. Singer, M. E. Pettit, Th. Nisius, Th. Wilhein, C. Gutt, G. Grübel, N. Guerassimova, R. Treusch, J. Feldhaus, S. Eisebitt, E. Weckert, M. Grunze, A. Rosenhahn and I. A. Vartanyants, "Coherent imaging of biological samples with femtosecond pulses at the free-electron laser FLASH," New J. Phys. **12**, 035003 (2010).
7. I. A. Vartanyants, A. P. Mancuso, A. Singer, O. M. Yefanov, and J. Gulden, "Coherence measurements and coherent diffractive imaging at FLASH," J. Phys. B: At. Mol. Opt. Phys. **43**, 194016 (2010).
8. T. Salditt, "Thermal fluctuations and stability of solid-supported lipid membranes," J. Phys.: Condens. Matter **17**, R287–R314 (2005).
9. C. R. Safinya, D. Roux, G. S. Smith, S. K. Sinha, P. Dimon, N. A. Clark, and A. M. Bellocq, "Steric Interactions in a Model Multimembrane System: A Synchrotron X-Ray Study," Phys. Rev. Lett. **57**, 2718–2721 (1986).
10. I. Sikharulidze, B. Farago, I. P. Dolbnya, A. Madsen, and W. H. de Jeu, "Surface and Bulk Elasticity Determined Fluctuation Regimes in Smectic Membranes," Phys. Rev. Lett. **91**, 165504 (2003).
11. D. Constantin, G. Brotons, T. Salditt, E. Freyssingeas, and A. Madsen, "Dynamics of bulk fluctuations in a lamellar phase studied by coherent x-ray scattering," Phys. Rev. E **74**, 031706 (2006).
12. J. Feldhaus, E. L. Saldin, J. R. Schneider, E. A. Schneidmiller, M. V. Yurkov, "Possible application of X-ray optical elements for reducing the spectral bandwidth of an X-ray SASE FEL," Opt. Commun. **140**, 341–352 (1997).
13. Z. Huang and K.-J. Kim, "Review of x-ray free-electron laser theory," Phys. Rev. ST Accel. Beams **10**, 034801 (2007).
14. I. A. Vartanyants, A. Singer, A. P. Mancuso, O. M. Yefanov, A. Sakdinawat, Y. Liu, E. Bang, G. J. Williams, G. Cadenazzi, B. Abbey, H. Sinn, D. Attwood, K. A. Nugent, E. Weckert, T. Wang, D. Zhu, B. Wu, C. Graves, A. Scherz, J. J. Turner, W. F. Schlotter, M. Messerschmidt, J. Lüning, Y. Acremann, P. Heimann, D. C. Mancini, V. Joshi, J. Krzywinski, R. Soufli, M. Fernandez-Perea, S. Hau-Riege, A. G. Peele, Y. Feng, O. Krupin, S. Moeller, and W. Wurth, "Coherence Properties of Individual Femtosecond Pulses of an X-Ray Free-Electron Laser," Phys. Rev. Lett. **107**, 144801 (2011).
15. J. Goodman, *Statistical Optics* (Wiley, 1985), Chaps. 4 and 7.
16. I. A. Vartanyants and A. Singer, "Coherence properties of hard x-ray synchrotron sources and x-ray free-electron lasers," New J. Phys. **12**, 035004 (2010).
17. A. Singer, I. A. Vartanyants, M. Kuhlmann, S. Duesterer, R. Treusch, and J. Feldhaus, "Transverse-Coherence Properties of the Free-Electron-Laser FLASH at DESY," Phys. Rev. Lett. **101**, 254801 (2008).
18. B. Schäfer, B. Flöter, T. Mey, P. Juranic, S. Kapitzki, B. Keitel, E. Pönjes, K. Mann, K. Tiedtke, "FEL beam characterization from measurements of the Wigner distribution function," Nucl. Instr. and Meth. A **654**, 502–507 (2011).
19. C. Gutt, P. Wochner, B. Fischer, H. Conrad, M. Castro-Colin, S. Lee, F. Lehmkühler, I. Steinke, M. Sprung, W. Roseker, D. Zhu, H. Lemke, S. Bogle, P. H. Fuoss, G. B. Stephenson, M. Cammarata, D. M. Fritz, A. Robert, and G. Grübel, "Single Shot Spatial and Temporal Coherence Properties of the SLAC Linac Coherent Light Source in the Hard X-Ray Regime," Phys. Rev. Lett. **108**, 024801 (2012).
20. A. Singer, F. Sorgenfrei, A. P. Mancuso, N. Gerasimova, O. M. Yefanov, J. Gulden, T. Gorniak, T. Senkbeil, A. Sakdinawat, Y. Liu, D. Attwood, S. Dziarzhytski, D. D. Mai, R. Treusch, E. Weckert, T. Salditt, A. Rosenhahn, W. Wurth, and I. A. Vartanyants, "Spatial and temporal coherence properties of single free-electron laser pulses," Opt. Express. **20**, 17480–17495 (2012).
21. W. F. Schlotter, F. Sorgenfrei, T. Beeck, M. Beye, S. Gieschen, H. Meyer, M. Nagasono, A. Föhlisch, and W. Wurth, "Longitudinal coherence measurements of an extreme-ultraviolet free-electron laser," Opt. Lett. **35**, 372–374 (2010).
22. S. Roling, B. Siemer, M. Wöstmann, H. Zacharias, R. Mitzner, A. Singer, K. Tiedtke, and I. A. Vartanyants, "Temporal and spatial coherence properties of free-electron-laser pulses in the extreme ultraviolet regime," Phys. Rev. ST Accel. Beams **14**, 080701 (2011).
23. K. Tiedtke, A. Azima, N. von Bargen, L. Bittner, S. Bonfigt, S. Düsterer, B. Faatz, U. Frühling, M. Gensch, Ch. Gerth, N. Guerassimova, U. Hahn, T. Hans, M. Hesse, K. Honkavaar, U. Jastrow, P. Juranic, S. Kapitzki, B. Keitel, T. Kracht, M Kuhlmann, W. B. Li, M. Martins, T. Nunez, E. Plönjes, H. Redlin, E. L. Saldin, E. A. Schneidmiller, J. R. Schneider, S. Schreiber, N. Stojanovic, F. Tavella, S. Toleikis, R. Treusch, H. Weigelt, M.

#186355 - $15.00 USD Received 8 Mar 2013; revised 11 Apr 2013; accepted 11 Apr 2013; published 20 May 2013

Wellhöfer, H. Wabnitz, M. V. Yurkov, and J. Feldhaus, "The soft x-ray free-electron laser FLASH at DESY: beamlines, diagnostics and end-stations," New J. Phys. **11**, 023029 (2009).
24. F. Staier, "Entwicklung, Bau und Test einer UHV Röntgenstreukammer für die digitale In-Line Holographie," Ph.D. Thesis, University of Heidelberg (2009).
25. M. Braeuer, U. Hahn, and S. Toleikis, "A mechanical shutter to select single bunch trains at the FLASH facility at DESY," Proccedings FEL 2006.
26. E. L. Saldin, E. A. Schneidmiller, and M. V. Yurkov, "Self-amplified spontaneous emission FEL with energy-chirped electron beam and its application for generation of attosecond x-ray pulses," Phys. Rev. ST Accel. Beams **9**, 030702 (2006).
27. T. L. Alexander, J. E. Harvey, and A. R. Weeks, "Average speckle size as a function of intensity threshold level: comparisonof experimental measurements with theory," Appl. Opt. **33**, 8240–8250 (1994).
28. Ch. Morawe, M. Osterhoff, "Hard X-Ray Focusing with Curved Reflective Multilayers," NIM A 616, 98–104 (2010).
29. M. Osterhoff, T. Salditt, "Coherence filtering of x-ray waveguides: analytical and numerical approach," New J. Phys. **13**, 103026 (2011).
30. M. Orsi, J. Michel, and J. W. Essex, "Coarse-grain modelling of DMPC and DOPC lipid bilayers," J. Phys.: Condens. Matter **22**, 155106 (2010).
31. C. Li, "Strukturanalyse von antibiotischen Peptiden in Lipidmembranen mittels Röntgen-reflektivität," Ph.D. thesis, University of Göttingen (2004).
32. B. L. Henke, E. M. Gullikson, and J. C. Davis, "X-ray Interactions: Photoabsorption, Scattering, Transmission, and Reflection at E = 50-30,000 eV, Z = 1-92," Atomic Data and Nuclear Data Tables **54/2**, 181–342 (1993).

## 1. Introduction

The so-called water window spectral range of soft X-rays in between the absorption edges of carbon (4.37 *nm*) and oxygen (2.33 *nm*) is of particular relevance for X-ray microscopy and imaging of biological samples [1–3]. The relatively strong interaction with matter, in particular for biomolecular samples consisting of low Z elements, in combination with sufficient transparency of a few microns in aqueous media enables high resolution structural analysis enhanced by spectroscopic sensitivity around several relevant absorption edges. Highly coherent femtosecond X-ray pulses have now become available for single pulse diffraction and imaging due to the advent of Free-Electron laser (FEL) radiation [4, 5]. As the FLASH facility at DESY, Hamburg, has shifted operation to shorter wavelength the water window has become accessible [6, 7]. In this work we use the FLASH third harmonic to probe a stack of multilamellar lipid membranes [8] with a periodicity of $d \simeq 5$ *nm* using single pulse diffraction. The lateral domain structure of the aligned membranes as well as the height fluctuations of membranes lead to a random phase variation of the exit wave, giving rise to a pronounced speckle pattern at and around the first lamellar Bragg peak. Note that the pronounced thermal height fluctuations in the lamellar stack typical for smectic liquid crystals are probed quasi-instantaneously in this scheme by a pulse length in the range of 100 $fs$. As a result, the diffraction pattern does not average out to a smooth lineshape as in conventional experiments [9–11]. As the high spatial coherence of the X-ray pulses is one of the key properties of Free-Electron Laser radiation [12–14], in particular for applications of single pulse coherent X-ray imaging, we have analyzed the recorded speckle patterns in view of the spatial coherence properties, similar to the statistical optics approach by Goodman [15].

Coherence and wavefront properties of FEL pulses generated by self-amplified spontaneous emission (SASE) have been considered before in detail both, theoretically [16] and experimentally [17–19]. Different strategies to measure coherence properties have been used: (i) double slit and pinhole experiments [14, 17, 20] and extensions to uniform redundant arrays [7], (ii) interference of two time-delayed beams [21, 22], (iii) Hartmann wavefront sensors [18], and (iv) coherent diffraction from random media and subsequent speckle analysis [19]. Some of the above approaches are difficult or impossible to perform for single pulses, which is significant as the effective coherence properties may appear reduced by averaging over several pulses. For third harmonic radiation measurements, the suppression of the fundamental is a further is-

#186355 - $15.00 USD Received 8 Mar 2013; revised 11 Apr 2013; accepted 11 Apr 2013; published 20 May 2013

sue which must be addressed. Here we use the approach of speckle analysis and randomized phase fronts, as a simple and robust approach to extract the global degree of coherence, compatible with single pulses and selected sensitivity to the 3rd harmonic. Furthermore, as a first step of subsequent studies of structural dynamics it is important to disentangle effects of beam coherence and sample structure by analyzing the diffraction pattern. To this end, we use the highly aligned phospholipid membrane stacks as a well-controlled soft matter model systems. We restrict ourselves to studies of lateral (spatial) coherence, since these are most important for imaging and X-ray photon correlation spectroscopy (XPCS). Finally, beyond the issue of coherence, we also show that the diffraction signal corresponding to the $d = 5\ nm$ inter membrane spacing can be recorded using FLASH's third harmonic in a single pulse, with sufficient signal for quantitative analysis. The speckle pattern reflects the instantaneous state of the lipid membranes, without the temporal average over dynamic modes (undulations), since the femtosecond pulse duration is much shorter than any collective dynamics of membranes.

## 2. Experimental details

The experiment was carried out using beamline BL2 at FLASH with the following parameters: fundamental wavelength of $\lambda_{fund} = 8\ nm$, pulse energy $\simeq 220\ \mu J$, pulse duration $\simeq 100\ fs$, and repetition rate 10 Hz. To suppress the fundamental with respect to the 3rd harmonic ($\lambda_{3rd} = 2.66\ nm$) used for the coherent diffraction experiment, two Silicon filters of 216 *nm* and 273 *nm* thickness were used, with attenuation factors of $T_{fund}^{216nm} = 0.9\%$ / $T_{3rd}^{216nm} = 55.1\%$ and $T_{fund}^{489nm} = 0.0024\%$ / $T_{3rd}^{489nm} = 25.9\%$, respectively. Following two flat mirrors, the FEL was focused by an ellipsoidal C-coated mirror at 73 *m* distance from the SASE source. In [23], a typical focal beam size at the sample position of about $F_d = 20\ \mu m$ (FWHM) was reported. During the present measurement campaign, the focal size of the fundamental was determined to ($F_{fund} = 10(2)\ \mu m$) [20] using PMMA imprints. For the third harmonic, speckle size analysis gave $L_{3rd}^{x} = 6.2(9)\ \mu m$ and $L_{3rd}^{y} = 2.3(3)\ \mu m$, for the horizontal and vertical direction, respectively, as presented in detail in section 4.

Figure 1 shows a schematic of the FEL beam impinging at an incidence angle $\alpha_i$ onto the vertically oriented multilamellar stack of 1,2-Dioleoyl-sn-glycero-3-phosphocholine (DOPC) lipid membranes, deposited on Silicon substrates [8], which were placed on multiple sample holders in the high vacuum diffraction chamber [24], housing the (i) differential pumping stage providing high vacuum condition, (ii) optical telescope for in-situ observation during measurements and for adjustment of stepper position, ( iii) motorized sample and CCD stages for the corresponding measurement setups (transmission and reflection geometry), and (iv) the CCD detector (Andor DODX436-BN back-illuminated X-ray CCD camera, $2048 \times 2048$ pixels, with pixel size $13.5 \times 13.5\ \mu m^2$).

The periodicity $d = 5.06(6)\ nm$ of the multilamellar lipid stacks was determined from the Bragg reflection of the 3rd harmonic at $2\theta = 31.2(4)^\circ$. Considering an attenuation length of 218 *nm* for DOPC at the photon energy of $E_{3rd} = 525.7\ eV$ and the angle of incidence, a set of 22 lipid bilayers is contribution to the diffraction signal, see appendix (section 8) for details. The distance between sample and detector was $\Delta X = 8.42\ cm$. The angular fluctuation of the Bragg peak with standard variation of $\pm 5$ x-pixels (0.69 mrad) and $\pm 4$ y-pixels (0.55 mrad), respectively, can be explained by the pulse-to-pulse fluctuation of the FEL beam. This will be discussed in detail in the next section. The specular Bragg peak is accompanied by pronounced tails of diffuse scattering in conventional incoherent diffraction, forming a so-called Bragg sheet. Here it appears as a highly speckled intensity distribution with a Gaussian envelope, see Figs. 2 and 3. The entire coherent intensity distribution of the first order Bragg peak/sheet was recorded at high oversampling conditions for the speckles. Using $T_{fund}^{216nm}$, a single pulse recording exhibits a signal level of up to a factor of 7-8 above background (read out noise), entirely

#186355 - $15.00 USD Received 8 Mar 2013; revised 11 Apr 2013; accepted 11 Apr 2013; published 20 May 2013

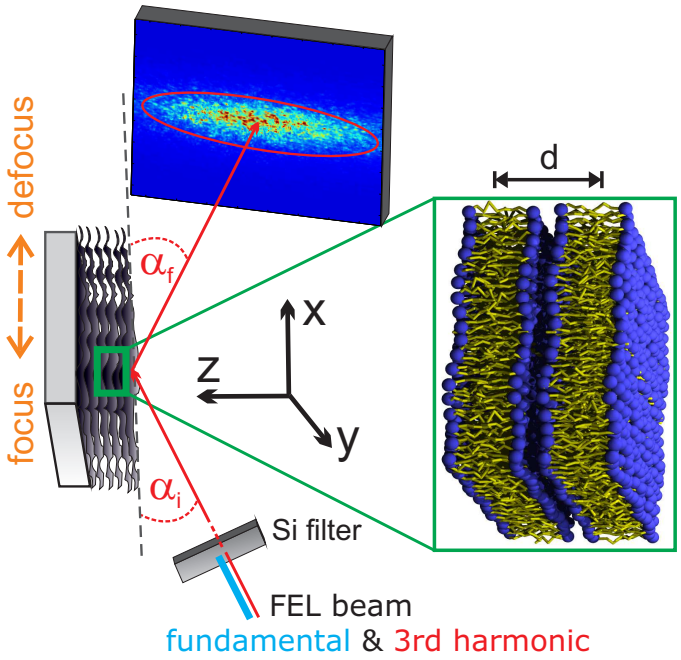


Fig. 1. Schematic of the measurement setup for coherent diffraction of DOPC lipid membrane multilayers using the FEL 3rd harmonic ($\lambda_{3rd} = 2.66$ *nm*). FEL intensity on the sample is controlled by two attenuating Si-foils (216 *nm* and 289 *nm*). At an incidence angle of $\alpha_i = 15.6°$, the first order Bragg sheet of the membrane stack (specular peak surrounded by speckles corresponding to the diffuse Bragg sheet) is recorded by a CCD detector. By shifting the sample from the focal position to a defocus position, the size of the illuminated area can be increased.

attributed to the 3rd harmonic, since the multilamellar acts as a monochromator, used in addition to the 216 *nm* Si filter. In the single pulse operation, a mechanical shutter was used to select single bunches of the FEL beam, moved by a low-voltage motor which starts 100 ms before the next bunch. The programmable logic controller (PLC) triggers the open-close mechanism and provides IO-modules, e.g. the selected bunch identification numbers. In the described experiment, the CCD camera software sends a bunch request to the PLC. Further information can be found in [25].

Accumulation of further pulses on the same sample spot shows only a sharp specular reflection (Fresnel reflectivity) of the bare substrate, showing that the multilamellar sample is destroyed within one shot at these conditions denoted as the low-att./focus setting below, see Fig. 2(a). Interestingly, by use of both filters, the combined attenuation of the fundamental $T_{fund}^{489nm} = 0.0024\%$ is sufficient to prevent this damage, and reproducible diffraction patterns can be accumulated, however at much weaker single pulse signal levels, see Fig. 2(b). Note that in this case, the sample was also translated by 3 *cm* along the optical axis from a focal ($\Delta X_{foc}^{CCD} = 8.4$ *cm*) to a defocal ($\Delta X_{defoc}^{CCD} = 5.4$ *cm*) position, which leads to a larger FEL beam size, as evidenced by correspondingly smaller speckle size. These high-att./defocus series shown in Fig. 2(b) exhibits marginal changes in the peak position and intensity. However, the speckle intensity distribution which is dominant in the low-att./focus series is washed out by photon shot noise. The option to switch between both measurement modes by simple choice of attenuators and sample distance is an important advantage of the used experimental design.

#186355 - $15.00 USD Received 8 Mar 2013; revised 11 Apr 2013; accepted 11 Apr 2013; published 20 May 2013

## 3. FEL pulse-to-pulse variation

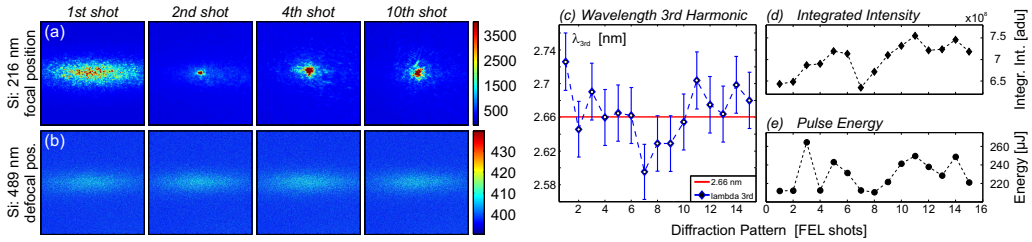


Fig. 2. (a) Successive single pulse diffraction patterns recorded from the same spot on the sample, using the low-att./focus setting. The series shows that the multilamellar sample is destroyed within one shot (diffract & destroy principle). Contrarily, under high-att./defocus conditions, the flux density of the fundamental is sufficiently low to prevent this damage. Diffraction images shown in (b) exhibit no radiation induced changes within the series of 10 recordings. However, the single pulse signal level is much weaker and thus not suitable for speckle analysis. Series (a) was used to determine the Bragg angle $2\theta$ for each shot. From the mean Bragg angle and $\lambda_{3rd} = 2.66$ *nm*, the periodicity $d$ of the membrane stack was calculated. The pulse-to-pulse variation of the incidence angle of 0.5% (rms) is attributed to fluctuations in $\lambda_{3rd}$. (c,d,e) The graphs show the wavelength ($\lambda_{3rd}$) (based on $d = 5.06(6)$ *nm*), the integrated intensity of the Bragg peak, and the energy of the electron bunch, respectively, for each pulse.

Next, we consider the pulse-to-pulse variations of the diffraction patterns, as recorded under the low-att./focus setting. Evaluating the peak position (by fitting the corresponding envelope along $q_z$, see Fig. 3) for each shot recorded at a new sample position, we can assume that the lamellar periodicity $d$ is constant. Note that $d$ is set by the equilibrium of molecular forces. While the total number of bilayers may vary across the sample, we know from previous measurements (with hard x-rays) that $d$ is constant, within one sample, and between equivalent samples under the same environmental conditions. From the mean peak position (averaged over 15 pulses), we get $d = 5.06(6)$ *nm*. As no excitation of the membrane layers is given, the variation in $d$ can be understood as pulse-to-pulse variations, which is attributed to wavelength fluctuations of the FEL's 3rd harmonic beam. The corresponding values of the wavelength $\lambda_{3rd}$ and the integrated intensities of the single pulse Bragg sheets are shown in Fig. 2(c), and (d), respectively. Note that the data points do not correspond to successive pulses, but were recorded over a period of several hours. The observed standard deviation of the 3rd harmonic can be estimated to 1.24%, corresponding to an absolute value of $\sigma_{\lambda_{3rd}} = 0.033$ *nm*. This agrees very well with bandwidth measurements of the fundamental using the online spectrometer upstream of the beamlines, which gave an bandwidth of 1.1% (average over 100 spectra, standard variation), noted as 2.5% FWHM in the online accessable FLASH beamline logbook. These measurements were performed before and after the present experiment. Hence as expected [26], the bandwidth of the first and 3rd harmonic are identical within experimental errors. These fluctuations can impose a problem, e.g. for pump-probe experiments where only small changes of observables are expected after excitation, which can easily be masked by pulse-to-pulse fluctuations in photon energy.

## 4. Speckle pattern and coherence analysis

Next we address the lineshape and statistical properties of the single pulse coherent diffraction patterns of the first lamellar Bragg peak, as recorded under the low-att./focus setting described above. A typical diffraction pattern is shown in Fig. 3(a) as a function of $q_z$ and $q_y$, along

#186355 - $15.00 USD Received 8 Mar 2013; revised 11 Apr 2013; accepted 11 Apr 2013; published 20 May 2013

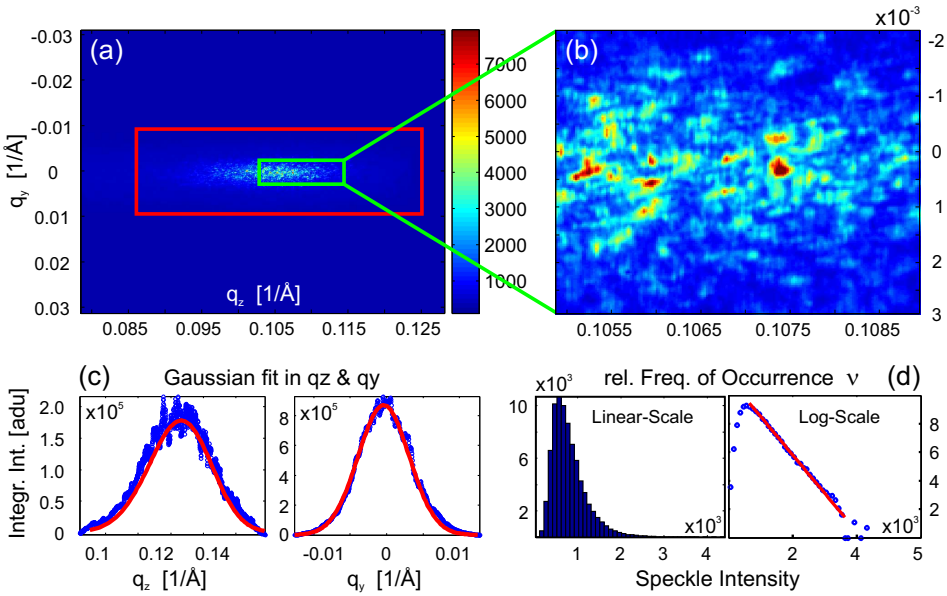


Fig. 3. (a) A typical first order Bragg sheet of the multilamellar membranes. (b) By zooming into the Bragg sheet (green ROI) a well sampled speckle pattern with a characteristic intensity distribution is visible. (c) The position and width of the Bragg sheet (red ROI) is determined by fitting the profile along the two principal axis to a Gaussian lineshape with linear background. (d) For statistical analysis the intensity values - corrected for background scattering - have been binned in intervals of 100 analog-digital units (adu), resulting in the experimental values of relative frequency of occurrence $\nu$. The right tail of the distribution exhibits an exponential lineshape, as evidenced by the linear plot on semi-log scale. The distribution is characteristic for the (spatial) coherence properties of the FEL beam.

with a corresponding zoom (b) in an enlarged sub-region of the peak showing the pronounced statistical speckle structure. Note that $q_z, q_y, q_x$ can be computed without approximation for each pixel from the scattering angles. However the iso-lines of $q_y$ are not exactly straight lines (horizontal lines in the CCD image) but exhibit slight curvature, which not taken into account in the plot of (a,b). Note that the resulting errors are smaller than 4%. More importantly, we do not need conversion from pixels to $\vec{q}$ for the individual pixels in the analysis, but only for the peak position and width. The mean speckle size derived from autocorrelation analysis of the coherent diffraction patterns along the two principal directions are $\Delta P_h \simeq 12(2)$ pixels in the horizontal and $\Delta P_v \simeq 8(1)$ pixels in the vertical direction, respectively. This gives access to the beam footprint on the sample. The corresponding angular width of the speckle is inversely proportional to the beam size $\Delta\beta = \lambda/L$ in the $y$ direction, with an additional factor of $\sin(\alpha_i)$ accounting for the projection of the beam along $x$ in the reflectivity plane. Accordingly, we get for the footprint of the beam $L_y = 2.3(3)\ \mu m$ and $L_x = 6.2(9)\ \mu m$, which can be compared to the results from beam imprint experiments on PMMA (see appendix for further details).

A speckle pattern emerges when a spatially coherent beam is reflected from any sort of disordered surface. Well known examples are the speckle patterns recorded from rough surfaces or disordered colloids. Indeed, a zoom in Fig. 3 exhibits the speckled nature of the diffraction pattern under Bragg condition, with a characteristic intensity distribution function. In particular, a number of pixels carry only marginal intensity. As can be shown in statistical optics [15], the most likely intensity value for interference from randomized object is zero, as resulting from

#186355 - $15.00 USD Received 8 Mar 2013; revised 11 Apr 2013; accepted 11 Apr 2013; published 20 May 2013

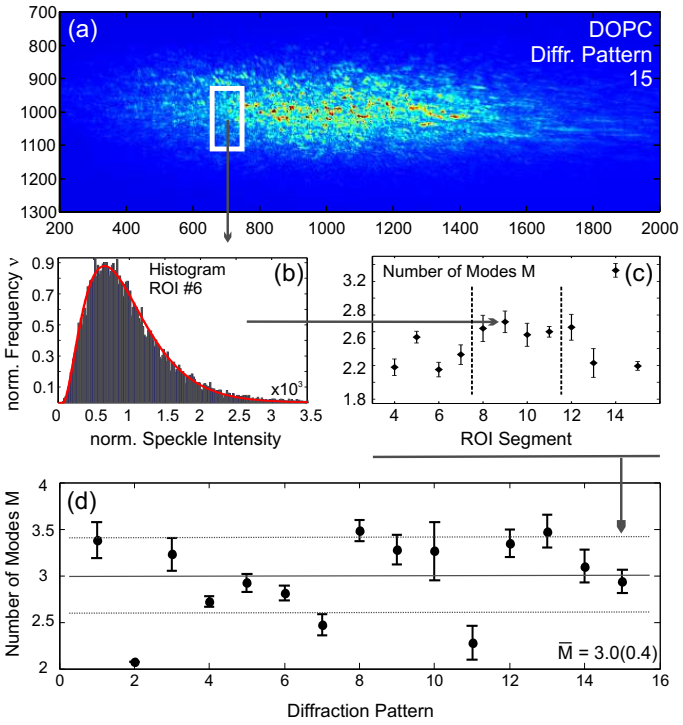


Fig. 4. (a) Diffraction pattern of the dataset DOPC-15, and (b) the corresponding histograms of a region of interest (ROI), as illustrative example for the analysis. The intensity distribution is in excellent agreement with the gamma probability distribution function, Eq. (1). (c) The resulting number of modes averaged over the ROI is then evaluated as a function of ROI position. Note that the low intensities in the tails of the peak lead to larger statistical errors, so that these ROIs are discarded and only the central ROI positions (in the Bragg sheet plateau) are kept for further analysis. (d) The mode number $M$ averaged over the central ROIs for each single shot data sets. The error of each data set is calculated from the standard deviation of the evaluated ROIs. The average over the entire ensemble of single shot data sets yields $\bar{M} = 3.0(4)$, quantifying the partial (spatial) coherence of the 3rd harmonic.

destructive interference, if and only if the beam is fully coherent. The distribution then falls off exponentially with $I$. Partial coherence or a finite number of modes lowers the frequency of occurrence of zero intensity, but can be shown to still exhibit an exponential tail at high $I$. The intensity histogram thus reveals important information on the global coherence, i.e. the global number of modes. According to [15, 27], a model for the intensity probability density function (PDF) $p(I)$ can be derived for diffraction intensities given as the squared modulus of a sum over independent Gaussian random fields, corresponding to the random phase shifts of a disordered sample

$$p(I) = \left(\frac{M}{\bar{I}}\right)^M I^{M-1} \frac{\exp\left[-M\,\frac{I}{\bar{I}}\right]}{\Gamma(M)}\,, \tag{1}$$

where $\bar{I}$ is the average intensity, $\Gamma(M)$ the gamma function and $M$ the number of modes. In the present case, (1) can be used to quantify the number of modes contained in a FEL pulse. As illustrated by the histogram, the distribution of intensity values shown for example in Fig. 3 indeed exhibits an exponential tail $p(I) \propto \exp(-I/I_e)$ with decay constant $I_e = 406$. The ran-

#186355 - $15.00 USD Received 8 Mar 2013; revised 11 Apr 2013; accepted 11 Apr 2013; published 20 May 2013

dom phase shifts inflicted by the sample within the illuminated area (see discussion of the focal width) can be attributed to all sources breaking lateral translation invariance in the system (undulations, domain boundaries, uneven number of bilayers, lamellar defects). The detailed study of these effects, possibly including a real-space reconstruction, would be extremely interesting in view of the physics of soft matter interfaces.

Figure 4 shows the results of fitting the frequency of occurrence $v$ to Eq. (1). The values $v$ have been calculated by counting the number of pixels with intensities falling into the range of the corresponding bin. After normalization to the average intensity $\bar{I}$, the model fits with the free parameter $M$ show excellent agreement with the data, see (b). The sub-division of the speckled Bragg sheet into small regions of interest (ROIs) along the $q_z$ direction shows no systematic variation, see (c), where the result of fitting Eq. (1) to the ROIs at different position along the diffraction pattern are shown. The absence of systematic variation is an indication that path length differences, occurring for $\alpha_f \neq \alpha_i$, do not influence the speckle statistics. We can therefore conclude that the present is not sensitive to longitudinal coherence, and is fully dominated by lateral coherence properties. Note that the tails of the Bragg sheet have been discarded for the high statistical errors in these regions, so that only the intensity rich central ROIs contribute to the average $M$. The result of all analyzed data sets is displayed in Fig. 4(d), proving that the $M$ values of the different data sets are very consistent. The individual error bars are determined from the standard deviation of the fitting results corresponding to the central ROIs of each data sets. The mode number averaged over all data sets is $\bar{M} = 3.0(4)$, indicating a partially coherent 3rd harmonic beam with approximately three modes. The FEL's fundamental has been previously analyzed [18, 20]. Averaging over many pulses, wavefront analysis has yielded a degree of spatial coherence $\gamma_{26nm} = 0.4$ [18] at $\lambda_{fund} = 26$ *nm*, corresponding to $M_{26nm} = 2.5$. Single pulses analysis based on double slits experiments at $\lambda_{fund} = 8$ *nm* [20], yielded $\gamma_V \simeq 0.7$ and $\gamma_H \simeq 0.6$, for the vertical and horizontal direction, corresponding to $M_V = 1.4$ and $M_H = 1.7$, hence a total number of modes of $M_{8nm} = 2.38$. Thus, the coherence of the fundamental (single pulse measurements) is only slightly higher than that of the 3rd harmonic. Importantly, $M_{2.66nm} = 3.0$ is sufficient for coherent diffraction with good speckle contrast and amenable to quantitative analysis.

## 5. Conclusion

Single shot intensity histograms of FEL speckle pattern are shown to be a suitable method to determine the global degree of spatial coherence. The particular oriented multi-lamellar sample chosen here offers the advantage that only the 3rd harmonic is selected by interference. Of course, the method cannot serve to extract the full coherence function of FEL radiation, i.e. functional dependence of the coherence function $\gamma(\vec{r}_2, \vec{r}_2)$. However, alternative approaches like Young's double slit experiments or wavefront measurements based on Hartmann sensors are also limited when used on single pulses. To yield complete information on the coherence function, several patterns or defocus distances need to be combined, which is incompatible with single pulse characterization. Analysis of the speckle intensity histogram also provides a rather robust approach which could routinely be analyzed for larger sets of data, and which averages over the spatial dimensions.

Beyond the issue of coherence, the present experiment also shows that single femtosecond pulse coherent diffraction of biomolecular assemblies is possible in the water window spectral range. The reciprocal space resolution is high enough to study the inter-membrane periodicity $d \simeq 5$ *nm*, and the scattering signal is strong enough to enable quantitative speckle analysis. The speckle pattern reflects the instantaneous lamellar disorder, possibly both static (domain structure) and dynamic (undulations) in nature. However, in contrast to conventional experiments the femtosecond data accumulation is much shorter than any collective dynamics within

#186355 - $15.00 USD Received 8 Mar 2013; revised 11 Apr 2013; accepted 11 Apr 2013; published 20 May 2013

the lipid membrane. An extension of the experiment to laser excited dynamics in lipid membranes has already been performed, and is presently under detailed analysis. Before turning to the membrane's structural dynamics, this work has first addressed the proper mode of data accumulation and the experimental constraints related coherent properties and photon energy jitter of the FEL 3rd harmonic, which must be taken into account in the following work.

## 6. Appendix A

**Wave Optical Simulation of FEL Focus** The focus size and depth of focus relevant for the experiment can be estimated based on the geometric parameters of the ellipsoidal carbon coated mirror installed at FLASH BL2, as given in Table 1 below.

Table 1. Parameters of ellipsoidal mirror at BL2 [23]. For a simple model of the beam propagation, the bold-marked parameters are used.

| | |
|---|---|
| semi major axis a | 36.5 m |
| semi minor axis b | 0.624 m |
| semi focal length d | 36.495 m |
| **source focal length** | 71 m |
| **image focal length** | 2 m |
| **incidence angle** | 87° |
| **effective mirror length** | 0.490 m |
| effective mirror width | 0.030 m |

As a first estimation of focus properties, we used a numerical simulation of the elliptical focusing mirrors [28]. A point-source is propagated onto points on the mirror surface, where Fresnel's coefficient of reflection is applied. The amplitude is then propagated further down using the Fresnel-Kirchhoff integral of diffraction to the focal region. The same algorithm was applied for individual point-sources placed along the extend of an assumed extended source, and then averaged [29]. The simulations for the point-source give a lower bound on the focus size, yielding a FWHM of about 0.57 $\mu m$ and a depth of focus of 1 *mm*. As a model for a rather large illumination, we have used a Gaussian beam with a source diameter of 150 $\mu$m (FWHM), yielding an upper bound for the focus size of 4.3 $\mu m$, and a depth of focus of 7 *mm*. Figure 5(a) shows the intensity in the focal region for the extended source; intensity cuts for the point-source (green lines) and the extended source (red dashed lines) are shown in parts (b, cut in the focal plane) and (c, cut along the optical axis).

## 7. Appendix B

**Speckle Analysis: Beam Footprint of the 3rd Harmonic** The coherent diffraction pattern with its characteristic speckle size can be used to derive the size of the sample illuminated by the FEL beam, for example in the case of a simple transmission experiment by the relation $\Delta q = 2\pi/L$, where $\Delta q$ and $L$ are the FWHM values of the speckle size (in reciprocal space) and of the illuminated footprint (in real space), respectively. Consider an angle of $\Delta 2\theta$ for a speckle size along the x-direction (horizontal CCD direction) and $\Delta\beta$ along the y-direction (vertical CCD direction), the reciprocal coordinates can be calculated using

$$\begin{aligned} \Delta q_x &= \frac{2\,\pi}{\lambda_{3rd}} \cdot \sin(\theta_B) \cdot \Delta 2\theta \;, \quad \text{with} \quad \Delta 2\theta = \left( \frac{\Delta P_h \cdot 13.5 \mu m}{D_{sd}} \right) \\ \Delta q_y &= \frac{2\,\pi}{\lambda_{3rd}} \cdot \Delta\beta \;, \quad \text{with} \quad \Delta\beta = \left( \frac{\Delta P_v \cdot 13.5 \mu m}{D_{sd}} \right) \;, \end{aligned}$$

#186355 - $15.00 USD Received 8 Mar 2013; revised 11 Apr 2013; accepted 11 Apr 2013; published 20 May 2013

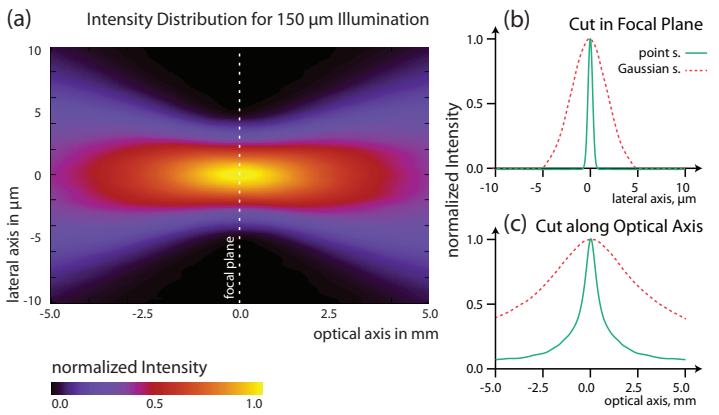


Fig. 5. FEL Beam propagation and focus simulations of the FLASH BL2 beamline, for the parameters of table 1. In (a), intensity of a Gaussian beam is shown in a focal region, for an designed extended source size of about 150 $\mu m$, as an upper limit for a numerical focus size estimation. On the right hand side, cuts of the simulated intensity are shown (b) in the focal plane and (c) along the optical axis. Green lines are for an assumed point-source, yielding a FWHM in the focus of about 0.57 $\mu m$; red dashed lines are for the assumed extended source (150 $\mu m$), yielding a FWHM of about 4.3 $\mu m$.

where $\Delta P_h$ and $\Delta P_v$ denote the speckle size (in pixel unit) in horizontal and vertical direction of the detector plane, and $D_{sd}$ the distance between sample and detector. The factor $\sin(\theta_B)$ takes account of the reflection geometry. In the following we calculate the average speckle size in horizontal and vertical direction on the CCD, corresponding to $L_x$ (parallel to optical axis) and $L_y$ (perpendicular to optical axis) in the sample plane. To this end, we calculate the auto-correlation of the background subtracted images, and determine the corresponding width (of the central peak) by calculation of its second moment $\sigma^{auto}$ along the two principal directions, see Fig. 6. Assuming a Gaussian speckle shape, we have to take into account a factor of $\sqrt{2}$ between the width of the speckle and the width of the autocorrelation function, which together with $FWHM = 2\sigma\sqrt{2 \cdot ln(2)}$ results in a full-width at half maximum (FWHM) value of

$$\Delta P_h = 2\sigma_{hor}^{auto}\ \sqrt{ln\,2} = 12(2) \text{ pixels}$$
$$\Delta P_v = 2\sigma_{vert}^{auto}\ \sqrt{ln\,2} = 8(1) \text{ pixels}\ .$$

Accordingly, we get for the focus size $L_x = 6.2(9)\ \mu m$ and $L_y = 2.3(3)\ \mu m$. This can be compared to results from PMMA imprint analysis [20], where imprints with several attenuation of the incoming beam were analyzed using the Gaussian beam profile to estimate the beam size. This beam profile analysis of the fundamental results in a beam width of $10(2) \times 10(2)\ \mu m^2$. Thus a 3rd harmonic beam width of $6.2(9) \times 2.3(3)\ \mu m^2$ lies within the range of expectation.

## 8. Appendix C

**DOPC Scattering Volume and Attenuation in the Sample** Next, we calculate the scattering volume, and in particular the number of illuminated membranes to estimate the entire film thickness of the multilamellar lipid bilayer stack.

Using the preparation parameters and the molecular volume and mass of DOPC according to [30], displayed in table 2, the entire thickness $D$ of the DOPC multilamellar stacks deposited

#186355 - $15.00 USD Received 8 Mar 2013; revised 11 Apr 2013; accepted 11 Apr 2013; published 20 May 2013

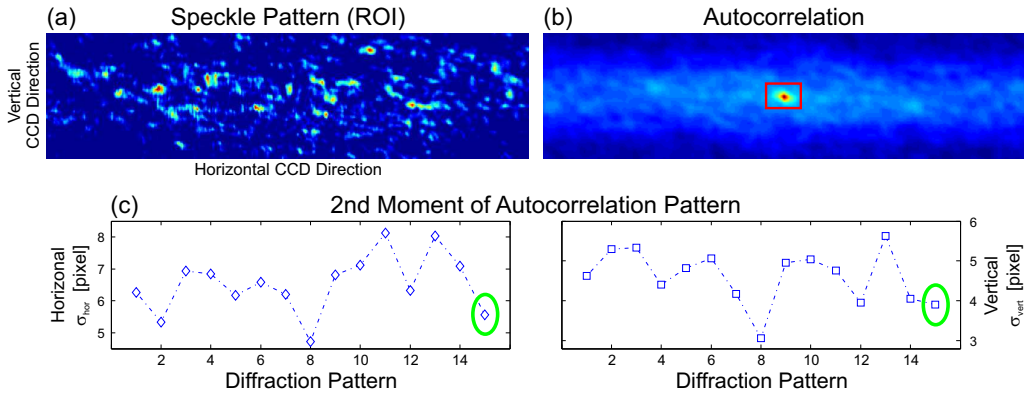


Fig. 6. (left, a) Zoom into the 15th speckle pattern, arising from Bragg diffraction of DOPC multilamellar stacks, shown as an example. The background (readout noise, residual scattering) as determined by a linear-fit of integrated intensities in horizontal and vertical axis was subtracted before the autocorrelation analysis. (left, b) The autocorrelation corresponding to (a) shown in linear scale. (right) Second moment of autocorrelation peak for different single pulse images, yielding an average of $\sigma_{hor}^{auto} = 7(1)$ pixels and $\sigma_{vert}^{auto} = 5(1)$ pixels along the horizontal and vertical axis, respectively.

Table 2. Parameters for the DOPC preparation.

| | |
|---|---|
| Concentration $c_L$ [mg/ml] | 15, 20 |
| Droplet volume on substrate $V$ [ml] | 0.05 |
| DOPC Molar mass [g/mol] | 786.113421 |
| Lipid volume $V_L$ [Å$^3$] | 1305.7 |
| Substrate surface area $A_{\text{sub}}$ [$mm^2$] | 100 |
| Bilayer thickness $d_{\text{DOPC}}$ [Å] | 50 |

on Si substrate can be calculated to [31]

$$D = \frac{c_L\, V\, N_A}{M_{\text{mol}}} \cdot \frac{V_L}{A_{sub}} \,.$$

With $N = \frac{D}{d_{\text{DOPC}}}$, the number of DOPC layers for the concentrations $c_L$ used in the experiment are given in the Table 3.

Table 3. DOPC total sample thickness and number of layers as a function of lipid concentration $c_L$.

| $c_L$ [mg/ml] | 15 | 20 |
|---|---|---|
| D [$\mu m$] | 7.5 | 10.0 |
| N [layers] | 1500 | 2000 |

Due to absorption, the FEL beam reaches only the top layers of the stack. From the absorption length calculated for DOPC at the given photon energy, see Fig. 7, and the fact that the FEL beam has to pass the layers twice in a reflection geometry, the top 108 *nm* of the film are illuminated ($1/e$ length), corresponding to 22 bilayers.

#186355 - $15.00 USD Received 8 Mar 2013; revised 11 Apr 2013; accepted 11 Apr 2013; published 20 May 2013

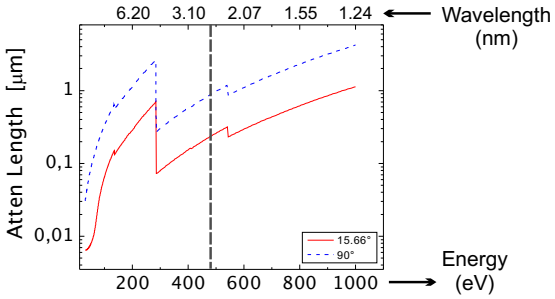


Fig. 7. Attenuation length of DOPC multilayers at incident angles of 15.6° ($1^{st}$ Bragg reflection for $\lambda_{\mathrm{FLASH}} = 2.66$ nm) and 90° (relevant for transmission measurements) incidence angle relative to the surface, calculated for the $C_{44}H_{84}NO_8P$ complex [32]. The resulting attenuation length for the FLASH $3^{rd}$ harmonic ($\lambda_{3\mathrm{rd}} = 2.66$ nm, $E_{3\mathrm{rd}} = 525.723$ eV) is $D_{2.66/15.6^\circ} = 218$ *nm* which corresponds to 43 DOPC bilayers.


## Acknowledgment

We thank the staff at HASYLAB/FLASH, and acknowledge support from the Deutsche Forschungsgemeinschaft through *SFB 755 Nanoscale Photonic Imaging*, BMBF Projects 05K10VH4 and 05K10CHG, as well as the Virtual Institute (Helmholtz Assoc.) VI-403.



#186355 - $15.00 USD Received 8 Mar 2013; revised 11 Apr 2013; accepted 11 Apr 2013; published 20 May 2013